Hysteresis, Period Doubling, and Intermittency at High Prandtl Number in the Lorenz Equations

By A. C. Fowler and M. J. McGuinness

We analyse a recently derived difference equation for the Lorenz equations, and thereby predict previously observed phenomena of period doubling and intermittent transitions. We also predict a hysteretic effect in such transitions, and give quantitative approximations to the bifurcation curves in (r, σ) parameter space. These are in agreement with the results of direct numerical simulation.

1. Introduction

The system of equations due to Lorenz [12] has been the subject of an enormous amount of recent research. The physical interest in these equations stems from the fact that in certain parameter regions, they exhibit "chaotic" behavior: solutions are aperiodic, and depend sensitively on the initial conditions. It was the possibility of similar qualitative behavior in atmospheric dynamics (and its relevance to the problem of long-range weather forecasting, for example) that originally stimulated Lorenz's interest, even though the set of three ordinary differential equations which he studied had no direct application to thermal convection, albeit derived from the equations describing that motion.

In a sense, Lorenz "explained" the aperiodic nature of solutions (and hence the sensitive dependence on initial conditions) by constructing (from his numerical solution) a difference equation (essentially a Poincaré map) which related successive maxima of one of the variables, Z.

In a different context (see May [18], Collet and Eckmann [3]), the study of difference equations of the form $x_{n+1} = af(x_n)$ with a bifurcation parameter a has shown that chaotic (aperiodic, etc.) sequences of the iterating variable are to be expected as the parameter a is increased, provided the iterating function f is hump-shaped. For small a, there is a unique nonzero steady state $af(x^*) = x^*$,

Address for correspondence: Professor A. C. Fowler, Room 2-336, M.I.T., Cambridge, MA 02139.

STUDIES IN APPLIED MATHEMATICS 69:99–126 (1983)

Published by Elsevier Science Publishing Co., Inc.
0022-2526/83/$3.00

and as a increases, this steady state successively bifurcates to a period-two cycle ($x_2 = f^2(x_2) \equiv f[f(x_2)]$), a period-four cycle ($x_4 = f^4(x_4)$), and so on until periodic cycles of all periods exist. The interval of a-values in which these bifurcations occur may be called a *period-doubling window*.

The bifurcation parameter in the Lorenz equations is called r, and similar period-doubling behavior can be observed. However, this does not happen as r increases (the obvious way would be by successive period-doubling bifurcation of limit cycles produced by a Hopf bifurcation at a critical value $r = r_T$, but this bifurcation is generally *subcritical*, and the limit cycles do not exist as r increases past r_T); rather, there exists at high r a unique stable limit cycle which may be explicitly described in terms of elliptic functions [21, 24]. As r *decreases*, this limit cycle (which would correspond to a fixed point in an appropriate Poincaré map, or Lorenz-type difference equation) undergoes period doubling until a chaotic régime is entered. This regime, however, is not that encountered when r increases through r_T. There are in fact a number of different periodic orbits which emerge as r is decreased, and which are then involved in period-doubling windows as r decreases further [19, 15, 16].

The question of where these various periodic orbits (the ones "created" by period doubling) go to is essentially answered by Robbins [21] and Yorke and Yorke [27], who show (numerically) that at a smallest value of $r = 13.926\ldots$ (with other parameters σ and b being those of Lorenz), a homoclinic orbit exists, and as a result of this, a "homoclinic explosion" [25] takes place in which infinitely many periodic orbits are created in the vicinity of the homoclinic orbit [7]. It is these periodic orbits which are later "annihilated" in the period-doubling windows.

In terms of Lorenz's difference equation, the above phenomena may be partially understood. His difference map has a pronounced cusp at a particular value of the abscissa M_n (the nth maximum of Z in a numerical solution). Lorenz recognized this as a sign of a previous very close approach in phase space of the trajectory to the unstable origin, and this observation has been analytically extended by Yorke and Yorke [27] and Fowler and McGuinness [4], and is implicit in the geometric model of Guckenheimer and Williams [7]: the cusp is associated with a trajectory which lies on the stable manifold of the origin, and thus with the appearance in the system of homoclinic orbits. Also, if a difference equation does describe the evolution of the solution, then it is no surprise that as the parameter r varies, period-doubling windows do occur (even though the Lorenz map is not hump-shaped).

Another property the Lorenz equations have is that of intermittency, which is concerned with a parameter value where a saddle-node bifurcation takes place [25]; that is, a stable and an unstable periodic orbit coalesce and disappear. Near such values (and where the limit cycles no longer exist), numerical solutions oscillate in the vicinity of the extinguished limit cycles for long ("laminar") phases, being interrupted by an occasional irregular ("turbulent") burst. Such language is reminiscent, probably intentionally so, of the phenomenon of intermittency in turbulent pipe flow, first observed by Reynolds [20] (see also Schlichting [23]), but experimentally is more relevant to convective intermittency, observed by Maurer and Libchaber [17] in experiments on liquid helium. Intermittency is also simply interpreted in terms of a difference equation which can be

described (near some particular value of M_n, say M^*) as $M_{n+1} = M_n + a(M_n - M^*)^2 + \varepsilon$, as ε increases through zero (if $a > 0$). After the disappearance of the limit cycles (fixed points $\approx M^*$) at $\varepsilon = 0$, the solutions may exhibit "intermittent" chaos, provided (for example) no other fixed point is stable. Tresser et al. [26] show that it is quite possible (for an appropriate difference equation) that if another fixed point *is* stable, then as ε (or r) is increased and decreased successively, hysteresis will occur. Lorenz maps at lower values of the parameter b show two or three cusps, and in these circumstances hysteresis *might* occur; and in fact Fowler and McGuinness [4] show (for example) that multiple stable behavior can occur at the same values of r, σ, b, namely $r = 110$, $\sigma = 100$, $b = 1$.

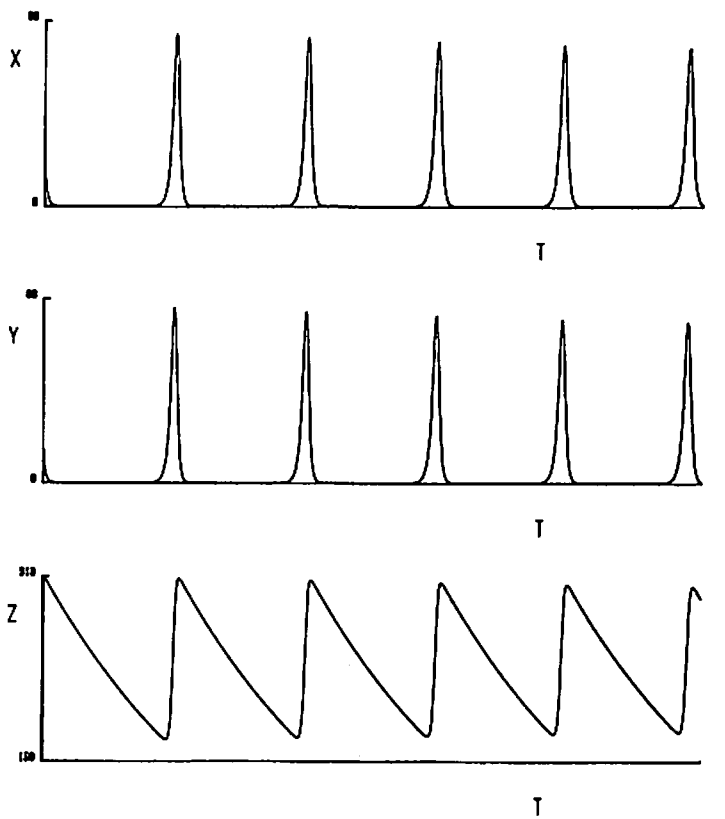

Figure 1. Transient solution at $\sigma = 300$, $r = 240$, $b = 1$. The trajectories are actually approaching one of the nontrivial fixed points at $X^2 = Y^2 = Z = 239$. Laser physicists will recognize the x and y plots as resembling the output of lasers [5, 9, 11], and it is known that weakly nonlinear amplitude equations for lasers are equivalent to the Lorenz equations [8, 6]; analogous spiking has also been obtained numerically in a higher-order model [2].

The three phenomena which form the title of this paper are thus all readily explicable in terms of an appropriate difference equation. The question now arises, why is it that a third-order set of differential equations should have an effectively one-dimensional Poincaré-type map, and in particular is it possible to explain for this map how the cusp is produced (and thus the wealth of bifurcation phenomena)? The answer to the first part of this question is well known, that is, that the Poincaré map is essentially one-dimensional (rather than two-dimensional) when the map is strongly contracting, and this is the case when the motion is relaxational in character. Levi [12] uses this relaxational character of the forced Van der Pol oscillator in the singular limit to construct analytically a one-dimensional Poincaré map. If we accept that the Lorenz map (or more strictly the Cantor set formed by its strange attractor) "looks" one-dimensional, then consistency suggests that we should utilize the relaxational character of the solutions which this implies to try and obtain an approximate analytic description of the map.

This program has been carried through in a previous paper [4]. We show there that the solutions are relaxational (see Figure 1) in the limit $r \sim \sigma \gg 1$, $b \sim 1$, and by asymptotic methods are able to directly "solve" the equations to obtain a Lorenz map with a large number of cusps. We feel this analysis illuminates in a constructive manner the mechanism by which chaotic solutions occur in this model. The purpose of this paper is to provide a partial analysis of the difference equation so obtained, and thus to identify and approximately locate regions in parameter space where the phenomena discussed above can occur, and to illustrate some of these predictions by numerical experiment.

2. A difference equation for the Lorenz equations

The Lorenz equations may be written in the following manner:

$$\begin{aligned} \dot{x} &= -x + y, \\ \dot{y} &= \rho(1-z)x - \delta\bar{\gamma}y, \\ \dot{z} &= xy - \delta z. \end{aligned} \tag{2.1}$$

Here a dot denotes differentiation with respect to time t. In terms of Lorenz's original variables X, Y, Z, τ, we have put

$$X = \sqrt{r\sigma}\,x, \quad Y = \sqrt{r\sigma}\,y, \quad Z = rz, \quad \tau = t/\sigma, \tag{2.2}$$

and the parameters ρ, $\bar{\gamma}$, δ are related to r, σ, b via

$$\rho = \frac{r}{\sigma}, \quad \delta = \frac{b}{\sigma}, \quad \bar{\gamma} = \frac{1}{b}. \tag{2.3}$$

The details of the rescaling and its motivation are explained by Fowler and McGuinness [4], and in this section we shall discuss an approximate difference equation relating successive maxima $\{M_n\}$ of the variable z, in the following asymptotic limit:

$$\rho = O(1), \quad \bar{\gamma} = O(1), \quad \delta \to 0, \tag{2.4}$$

corresponding to $r \sim \sigma \gg 1$, $b \sim 1$. For the sake of completeness, we sketch here the method of derivation, but would emphasize that for a complete analysis, reference must be made to our previous paper.

At leading order, then, as $\delta \to 0$, (2.1) has a first integral

$$\rho(1-z)^2 + y^2 = k^2/\rho$$

for some (as yet unspecified) $k = O(1)$. Solutions are thus

$$x \sim \frac{\dot{\phi}}{\sqrt{\rho}}, \quad y \sim -\frac{k}{\sqrt{\rho}}\sin\phi, \quad z \sim 1 + \frac{k}{\rho}\cos\phi,$$

where ϕ satisfies

$$\ddot{\phi} + \dot{\phi} + k\sin\phi = 0,$$

and represents a damped pendulum. Evidently this corresponds to the fast pulselike phase, and consideration of Figure 1 suggests matching

$$x, y \to 0, \quad z \sim m_n \quad \text{as} \quad t \to -\infty,$$

where $k = \rho(1 - m_n)$; alternatively $\phi \to \pi$ as $t \to -\infty$ (not 0, as this would be stable, and only the trivial solution would occur). Evidently m_n is approximately the minimum of z before the pulse, and then the subsequent maximum M_n is given by

$$M_n \sim 2 - m_n.$$

Now as $t \to \infty$, we have $\phi \to 0$, and so $x, y \to 0$, and thus the term δz in (2.1) becomes significant. We enter a slow phase, in which $z \sim M_n e^{-\tau}$, where $\tau = \delta t$, and x satisfies (approximately) the *linear* equation

$$\ddot{x} + \dot{x} + \rho(M_n e^{-\tau} - 1)x = 0,$$

where still $\dot{x} \equiv dx/dt$. This can actually be solved exactly (in terms of Bessel functions), but it is instructive to do so asymptotically (since this is what we are in

any case interested in). Independent solutions are

$$x \sim \exp\left[\frac{\lambda(\tau)}{\delta}\right],$$

where (ignoring $\delta\lambda''$), λ satisfies

$$\lambda'^2 + \lambda' + \rho\left[M_n e^{-\tau} - 1\right] = 0,$$

i.e.

$$\lambda' = -\tfrac{1}{2} \pm \tfrac{1}{2}\left[1 - 4\rho\left(M_n e^{-\tau} - 1\right)\right]^{1/2}.$$

Evidently, for $\tau \to 0$, both λ' are negative ($k > 0$, so $m_n < 1$, so $M_n > 1$): x decays towards zero coming out of the fast phase. For larger τ, one λ' remains negative, but the other becomes positive, so that this λ ultimately dominates, that is, $x \sim \exp[\lambda(\tau)/\delta]$, where

$$\lambda' = -\tfrac{1}{2} + \tfrac{1}{2}\left[1 - 4\rho\left(M_n e^{-\tau} - 1\right)\right]^{1/2}.$$

Eventually, despite having been exponentially small, x becomes of $O(1)$ again when $\tau = \tau^*$, say; we can choose τ^* by $\lambda(\tau^*) = \lambda(0)$ (if $M_n < 1 + 1/4\rho$), or

$$\tau^* = \int_0^{\tau^*} \left[1 - 4\rho\left(M_n e^{-\tau} - 1\right)\right]^{1/2} d\tau.$$

But now when $\tau = \tau^*$, we have $z \sim M_n e^{-\tau^*} \sim m_{n+1}$, since we are entering the next fast pulse. Thus the *next* maximum of z will be $M_{n+1} \sim 2 - m_{n+1}$, and thus we attain a leading-order difference equation of the form

$$M_{n+1} = 2 - M_n e^{-\tau^*},$$

$$\tau^* = \int_0^{\tau^*} \left[1 - 4\rho\left(M_n e^{-\tau} - 1\right)\right]^{1/2} d\tau.$$

The relation of the above equations to the more detailed result below will be opaque; we have only explained the methodology. To go to higher terms in δ, and to include detailed matching between solutions, we refer to [4]. Particularly, consideration of a distinguished intermediate limit is necessary when $M_n - (1 + 1/4\rho) \sim \delta^{2/3}$, and it is in this limit that we derive the particular form of

difference equation which is now reproduced:

$$M_n' = 1 + \frac{1}{4\rho} + \frac{\delta^{2/3}(1+4\rho)^{2/3}}{2^{4/3}\rho}\mu + \frac{\delta}{2\rho}\left[(1+4\rho)(1+\tfrac{1}{2}\theta) - \bar{\gamma}\right] + O(\delta^{4/3}),$$

$$M_n = M_n'\left[1 - \delta\chi(m_n, \rho) + O(\delta^2)\right],$$

$$m_n = 2 - M_n + O(\delta),$$

$$M_{n+1} = \left[2 - M_n' e^{-\tau^*}\right]\left[1 - \delta\chi(m_{n+1}, \rho) + \cdots\right] + \delta D(\bar{\gamma}, m_{n+1}, \rho) + O(\delta^2),$$

$$m_{n+1} = M_n' e^{-\tau^*} = \left(1 + \frac{1}{4\rho}\right)\operatorname{sech}^2\alpha^*, \tag{2.5}$$

$$\omega^* = \tfrac{1}{2}(1+4\rho)^{1/2}\tanh\alpha^*,$$

$$\tau^* = 2(1+4\rho)^{1/2}(\alpha^* - \tanh\alpha^*) - \delta\bar{\gamma}\left\{\frac{2\alpha^*}{(1+4\rho)^{1/2}} + \tau^*\right\}$$

$$+ 2\delta\ln\left[\left(\frac{\delta}{\pi\omega^*}\right)^{1/2}\frac{\pi a}{(\omega^* - \tfrac{1}{2})\delta^{2/3}2^{2/3}(1+4\rho)^{1/6}}\left|\mathrm{Ai}(-\mu)\right|\right] + O(\delta^{4/3}).$$

These are eight equations for the nine unknowns M_n', M_n, m_n, M_{n+1}, α^*, ω^*, τ^*, and μ, and thus constitute a difference equation for M_{n+1} as a function of M_n. They are valid for $|\mu| = O(1)$, i.e. $|M_n - (1 + 1/4\rho)| \sim \delta^{2/3} \ll 1$. The quantities $a, \theta, \chi(m, \rho)$, $D(\bar{\gamma}, m, \rho)$ are determined as follows: let $\phi(t; k)$ be the solution of

$$\ddot{\phi} + \dot{\phi} + k\sin\phi = 0,$$

$$\pi - \phi \sim \exp\left[\tfrac{1}{2}\left(-1 + (1+4k)^{1/2}\right)t\right], \qquad t \to -\infty, \tag{2.6}$$

$$k = \rho(1-m) \qquad (m < 1);$$

then

$$D(\bar{\gamma}, m, \rho) = (1-\bar{\gamma})(1-m)\int_{-\infty}^{\infty} \sin^2\phi\, dt$$

$$+ 2\left[\int_0^{\infty} \sin^2\left(\frac{\phi}{2}\right) dt - \int_{-\infty}^{0} \cos^2\left(\frac{\phi}{2}\right) dt\right]; \tag{2.7}$$

a, θ are defined by

$$\phi \sim a(\theta - t)e^{-t/2}, \quad t \to \infty, \qquad k = \tfrac{1}{4}; \tag{2.8}$$

and then χ is given by

$$\chi = t^* + \left[1 - \frac{2}{t^* - \theta}\right]^{-1}, \tag{2.9}$$

where t^* is the (larger) solution of

$$t^* = \ln\left[\frac{(1-m)a^2}{2(2-m)\delta}\right] + \ln\left[(t^*-\theta)^2 - 2(t^*-\theta)\right] + O(\delta^{2/3}), \tag{2.10}$$

(if δ is sufficiently small). Strictly, it follows [since $\chi \sim \ln(1/\delta)$] that $O(\delta^2)$ really means $O(\delta^2 \ln^2(1/\delta))$ in (2.5). Further, a, θ in (2.8) are (for $k = \frac{1}{4}$) a_0, θ_0 of [4], and thus use of these values in (2.10) engenders an error $O(\delta^{1/3})$ in t^*, and hence in χ. This gives an error of $O(\delta^{4/3})$ in M_n and M_{n+1}, which is, however, of no significance in the analysis which follows.

As it stands, (2.5) is very unwieldy; its use stems from the obvious fact that, by neglecting $O(\delta)$, one can obtain a much simpler form, whose behavior is qualitatively similar. This is

$$\begin{aligned} M_n &= 1 + \frac{1}{4\rho} + \frac{\delta^{2/3}(1+4\rho)^{2/3}}{2^{4/3}\rho}\mu, \\ M_{n+1} &= 2 - M_n e^{-\tau^*}, \\ M_n e^{-\tau^*} &= \left(1 + \frac{1}{4\rho}\right)\operatorname{sech}^2\alpha^*, \\ \tau^* &= 2(1+4\rho)^{1/2}(\alpha^* - \tanh\alpha^*) + 2\delta\ln|\mathrm{Ai}(-\mu)|. \end{aligned} \tag{2.11}$$

The last term in $(2.11)_4$ is retained because $\delta\ln|\mathrm{Ai}(-\mu)|$ is not uniformly small near zeros of $\mathrm{Ai}(-\mu)$. Equation (2.11) is valid to $O(\delta)$ [or $O(\delta\ln(1/\delta))$] for $\mu \sim 1$. For $|M_n - (1 + 1/4\rho)| = O(1)$, different formulae are appropriate, but they are not of immediate relevance. Away from zeros of $\mathrm{Ai}(-\mu)$, we can neglect the last term in $(2.11)_4$, and then the difference equation (and its continuation for $M_n < 1 + 1/4\rho$) is a continuous monotone increasing function, called the envelope difference equation.

When μ is near a zero of $\mathrm{Ai}(-\mu)$ (these are $\mu = |a_s|$, $s = 1, 2, \ldots$, where $a_1 = -2.338\ldots$, etc. [1], then $\mathrm{Ai}(-\mu) \approx -(\mu - |a_s|)\mathrm{Ai}'(a_s)$, $\tau^* \to \infty$, and we have

$$\begin{aligned} \tau^* &\approx 2(1+4\rho)^{1/2}(\alpha^* - 1) + 2\delta\ln|\mu - |a_s|| \\ &\approx 2(\alpha^* - \ln 2) + O(\delta^{2/3}) \end{aligned}$$

[from $(2.11)_3$]: therefore

$$\begin{aligned} M_{n+1} &\approx 2 - 4\left(1 + \frac{1}{4\rho}\right)e^{-2\alpha^*} \\ &\approx 2 - K|\mu - \mu_i|^\beta, \end{aligned} \tag{2.12}$$

where

$$\begin{aligned} \beta &= \frac{2\delta}{(1+4\rho)^{1/2} - 1}, \qquad \mu_i = |a_i|, \\ K &= 4\left(1 + \frac{1}{4\rho}\right)\exp\left[-\frac{2\{(1+4\rho)^{1/2} - \ln 2\}}{(1+4\rho)^{1/2} - 1}\right]. \end{aligned} \tag{2.13}$$

Equation (2.12) shows that for μ very close to $|a_s|$, narrow cusps occur superimposed on the envelope difference equation. The general picture is as shown in Figure 2, and this has been *directly confirmed numerically* (Figure 3).

It is easy to deduce from the approximate equations (2.11) that these cusps are *exponentially thin* in a well-defined sense [4]: the interval of M_n-values near $\mu = |a_s|$ for which $2 - M_{n+1} < K(1 - f)$ has width $\Delta_f \sim e^{-f/\beta}$, which for reasonable f is $\exp[-O(1/\delta)]$, since $\beta \sim \delta$. Further, cusps are spaced at $O(1)$ intervals of μ ($= |a_1|, |a_2|$, etc.) and thus at M_n intervals of $O(\delta^{2/3})$. On the other hand, minima between cusps occur for $\mu - |a_s| \sim O(\delta^{1/3})$, and for μ values much beyond this, the envelope approximation is valid: between cusps, this is [to $O(\delta^{2/3})$] simply a straight line. The local picture near a cusp is shown in Figure 4. For $M_n < 1 + 1/4\rho$, there are no cusps, and for $M_n > 1 + 1/4\rho$ ($\mu \gg 1$) the spacing

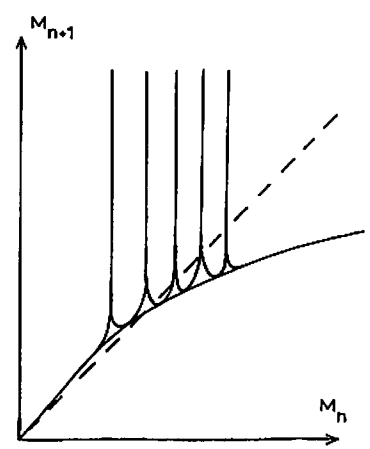

Figure 2. Schematic form of the Lorenz map (2.12).

between cusps decreases to $O(\delta)$. We shall not consider these regions further, as they are of little dynamical interest.

A little thought shows that interesting behavior occurs when a cusp is close to the fixed point of the envelope equation. Since "most" iterates M_n may be followed on the envelope (as the cusps are so thin), they will tend towards the envelope's fixed point. Only if this "nearly" coincides with a cusp will significantly different behavior occur. We can thus *define* a sequence of values ρ_s of ρ (which will depend on δ) such that for $\rho = \rho_s$, the sth cusp precisely overlies the fixed point of the envelope equation, say at C_s. Since $M_{n+1}(M_n)$ has a minimum at $C_s + O(\delta)$, one expects the "distinguished" limit to be $M_n = C_s + O(\delta)$, and hence $\rho = \rho_s + O(\delta)$: we might then hope to trace out the bifurcation structure as ρ changes in a small neighborhood of ρ_s.

It now becomes clear why we retained terms up to $O(\delta)$ in (2.5): although we could carry out the above program for (2.11), it cannot be expected to have numerical accuracy unless terms of $O(\delta)$ are included. We shall see that we

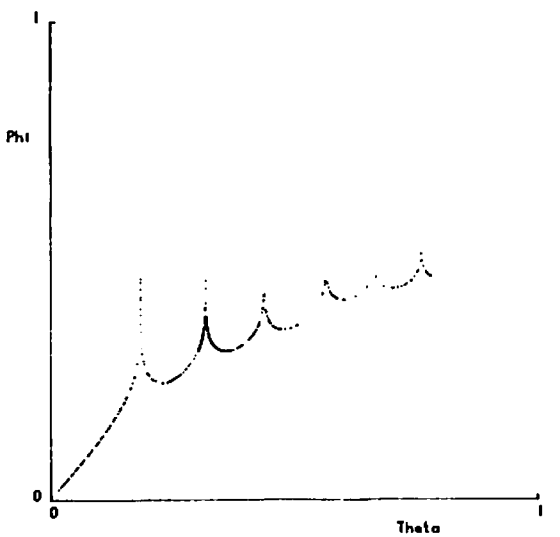

Figure 3. A numerically obtained difference map ($M_n = 1 + \theta$, $M_{n+1} = 1 + \phi$) at the parameter values $\sigma = 50$, $r = 100$, $b = 1$. (Stable behaviors at these parameters are T_1 f.p., $T_{1,2}$ ap.m. (see text).) Difference maps of the numerical solutions to the Lorenz equations are obtained by using many different initial values and by a "cusp-sharpening" algorithm that uses interval bisection on initial conditions to obtain values close to a desired cusp in the difference map. An essential requirement of this algorithm is to know whether a given point on the difference map is to the left or to the right of the cusp. This information is provided by our earlier results [4], which state, e.g., that if a point is to the left of the first cusp, then the number of zeros of x (or y) between the maxima of z which defines the point is zero; if the point is to the right, the number is one. The algorithm has been used to sharpen cusps to the left of the intersection(s) of the difference map with a 45° line, and could also be used on cusps to the right of this point.

cannot really expect great accuracy except for very small values of δ (which, however, are a little intractable for other reasons); we therefore retain such terms for reasons of consistency, even though the additional complexity does not alter the qualitative form of the results.

First, we define ρ_s to be the value of ρ for which the sth cusp overlies the fixed point of the envelope equation. The cusp is due to the term $|\mathrm{Ai}(-\mu)|$ in (2.5), and we may therefore define $\rho_s(\delta)$ as the value of ρ for which $M_{n+1} = M_n = C_s$, say, in (2.5) when this term is omitted; we then have $C_s = 1 + \frac{1}{4\rho} + O(\delta^{2/3})$, so $m_n \approx m_{n+1} = 1 - 1/4\rho + O(\delta^{2/3})$, and so, correct to $O(\delta)$, ρ_s is determined by

$$
\begin{aligned}
M_n' &= 1 + \frac{1}{4\rho} + \frac{\delta^{2/3}(1+4\rho)^{2/3}}{2^{4/3}\rho}|a_s| + \frac{\delta}{2\rho}\left[(1+4\rho)(1+\tfrac{1}{2}\theta) - \bar{\gamma}\right], \\
M_n &= C_s = M_n'[1 - \delta\chi^*(\rho)], \\
\chi^*(\rho) &= \chi\left(1 - \frac{1}{4\rho}, \rho\right), \\
M_{n+1} = C_s &= (2 - M_n' e^{-\tau^*})[1 - \delta\chi^*(\rho)] + \delta D^*(\bar{\gamma}, \rho), \\
D^*(\bar{\gamma}, \rho) &= D\left(\bar{\gamma}, 1 - \frac{1}{4\rho}, \rho\right), \\
M_n' e^{-\tau^*} &= \left(1 + \frac{1}{4\rho}\right)\mathrm{sech}^2\alpha^*, \\
\omega^* &= \tfrac{1}{2}(1+4\rho)^{1/2}\tanh\alpha^*, \\
\tau^* &= 2(1+4\rho)^{1/2}(\alpha^* - \tanh\alpha^*) \\
&\quad + 2\delta\left[\ln\left\{\left(\frac{\pi}{\omega^*}\right)^{1/2}\frac{\delta^{1/6}a|\mathrm{Ai}'(|a_s|)|}{(\omega^* - \frac{1}{2})2^{2/3}(1+4\rho)^{1/6}}\right\} - \bar{\gamma}\left\{\frac{\alpha^*}{(1+4\rho)^{1/2}} + \tfrac{1}{2}\tau^*\right\}\right].
\end{aligned}
\tag{2.14}
$$

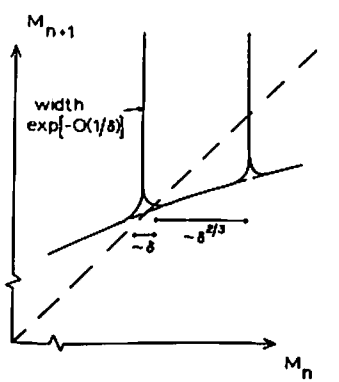

Figure 4. Cusp geometry for $|M_n - (1 + 1/4\rho)| \ll 1$.

We can simplify the above by dividing $(2.14)_{2,4}$ by $1-\delta\chi^*$: then

$$C_s' = \frac{C_s}{1-\delta\chi^*} = M_n' = 2 - M_n' e^{-\tau^*} + \delta D^* + \cdots, \tag{2.15}$$

and the last three equations in (2.14) are unchanged. Equations $(2.14)_{1,5,6,7,8}$ and (2.15) then constitute six equations for the unknowns D^*, ω^*, τ^*, α^*, M_n', ρ: we denote the corresponding values by D_s, ω_s, τ_s, α_s, C_s', ρ_s.

If μ varies by $O(\delta^{1/3})$, then M_n varies by $O(\delta)$, and so also τ^* and α^*: this engenders a balance with the term $\ln|\mathrm{Ai}(-\mu)|$ in (2.5). It is then appropriate to look at $O(\delta)$ variations in ρ, to determine the bifurcation behavior. Before doing so, we note the following. We are interested in a range $\mu \sim \delta^{1/3}$, or $\mu \ll 1$, i.e. $|M_n' - C_s'| \sim O(\delta)$; within this range the *envelope* value of M_{n+1}' ($\approx 2 - M_n' e^{-\tau^*}$) only varies by $O(\delta)$. The value of $M_{n+1}' - M_n'$ only exceeds $O(\delta^{2/3})$ in a thin region near C_s'. From previous remarks, the width of the region for which $M_{n+1}' - M_n' > O(f)$ [e.g. $M_{n+1}' - (2-K) \geq Kf$, i.e. $2 - M_{n+1}' \leq K(1-f)$] is $\Delta_f \sim e^{-f/\beta}$. When $f \sim \delta^{2/3}$, $\Delta_{\delta^{2/3}} \sim \exp[-1/(\delta^{1/3}\bar{\beta})]$, where $\bar{\beta} = \beta/\delta = 2/\{(1+4\rho)^{1/2} - 1\} = O(1)$. For small δ, $\Delta_{\delta^{2/3}}$ is thus exponentially small, and may be reasonably neglected (for the moment). In this case $|M_{n+1}' - M_n'| \lesssim \delta^{2/3}$ everywhere, and so we still have $m_n \approx m_{n+1} \approx 1 - 1/4\rho + O(\delta^{2/3})$; hence (for $|\mu - |a_s|| \gg \Delta_{\delta^{2/3}}$), we still have the approximations $\chi \approx \chi^*$, $D \approx D^*$, as before. Therefore we can again divide M_n and M_{n+1} by $1-\delta\chi^*$, and obtain, from (2.5),

$$\begin{aligned}
M_n' &= \left(1+\frac{1}{4\rho}\right) + \frac{\delta^{2/3}(1+4\rho)^{2/3}}{2^{4/3}\rho}\mu + \frac{\delta}{2\rho}\left[(1+4\rho)(1+\tfrac{1}{2}\theta) - \bar{\gamma}\right] + O(\delta^{4/3}),\\
M_{n+1}' &= 2 - M_n' e^{-\tau^*} + \delta D^*(\bar{\gamma}, \rho) + \cdots,\\
M_n' e^{-\tau^*} &= \left(1+\frac{1}{4\rho}\right)\mathrm{sech}^2\alpha^*,\\
\omega^* &= \tfrac{1}{2}(1+4\rho)^{1/2}\tanh\alpha^*,\\
\tau^* &= 2(1+4\rho)^{1/2}(\alpha^* - \tanh\alpha^*) + 2\delta\ln\left|\frac{\mathrm{Ai}(-\mu)}{\delta^{1/3}\mathrm{Ai}'(-\mu)}\right|\\
&\quad + 2\delta\left[\ln\left\{\left(\frac{\pi}{\omega^*}\right)^{1/2}\frac{\delta^{1/6}a|\mathrm{Ai}'(-\mu)|}{(\omega^* - \frac{1}{2})2^{2/3}(1+4\rho)^{1/6}}\right\} - \bar{\gamma}\left\{\frac{\alpha^*}{(1+4\rho)^{1/2}} + \tfrac{1}{2}\tau^*\right\}\right].
\end{aligned} \tag{2.16}$$

We now put

$$\begin{aligned}
\tau^* &= \tau_s + \delta\bar{\tau},\\
\alpha^* &= \alpha_s + \delta\bar{\alpha},\\
\rho &= \rho_s + \delta\bar{\rho},\\
\mu &= |a_s| + \delta^{1/3}\mu_n \qquad (\mu_{n+1} \text{ for } M_{n+1}'),
\end{aligned} \tag{2.17}$$

and expand, retaining terms up to $O(\delta)$ only. Omitting algebra, the result, correct to $O(\delta^{1/3})$, is

$$\begin{aligned}
p_1\mu_{n+1} - p_2\bar{\rho} &= p_3\bar{\rho} + p_4\bar{\alpha},\\
-C_s'\bar{\tau} + p_1\mu_n - p_2\bar{\rho} &= -p_5\bar{\rho} - p_6\bar{\alpha},\\
\bar{\tau} &= p_8\bar{\rho} + p_7\bar{\alpha} + 2\ln|\mu_n|,
\end{aligned} \tag{2.18}$$

where

$$\begin{aligned}
p_1 &= \frac{(1+4\rho_s)^{2/3}}{2^{4/3}\rho_s},\\
p_2 &= \frac{1}{4\rho_s^2},\\
p_3 &= p_2\mathrm{sech}^2\alpha_s,\\
p_4 &= 2\left(1+\frac{1}{4\rho_s}\right)\mathrm{sech}^2\alpha_s\tanh\alpha_s,\\
p_5 &= p_3 e^{\tau_s},\\
p_6 &= p_4 e^{\tau_s},\\
p_7 &= 2(1+4\rho_s)^{1/2}\tanh^2\alpha_s,\\
p_8 &= \frac{4(\alpha_s - \tanh\alpha_s)}{(1+4\rho_s)^{1/2}}.
\end{aligned} \tag{2.19}$$

From (2.18), we find the *canonical difference equation for* $\{\mu_n\}$,

$$\mu_{n+1} = \tilde{\rho} + \kappa\{\mu_n - \Omega\ln|\mu_n|\}, \tag{2.20}$$

where

$$\begin{aligned}
\tilde{\rho} &= \frac{\bar{\rho}}{p_1}\left[p_2 + p_3 + \frac{p_4(p_5 - p_2 - p_8C_s')}{p_7C_s' - p_6}\right],\\
\kappa &= \frac{p_4}{p_7C_s' - p_6},\\
\Omega &= \frac{2C_s'}{p_1}.
\end{aligned} \tag{2.21}$$

3. Bifurcation structure for the canonical difference equation

In this section we study the behavior of the equation

$$\mu_{n+1} = \tilde{\rho} + \kappa(\mu_n - \Omega \ln|\mu_n|), \tag{3.1}$$

as the bifurcation parameter $\tilde{\rho}$ is varied. Note that the derivation of (3.1) involves the (token) assumption that $\mu_{n+1} \lesssim O(\delta^{-1/3})$, which is valid away from an exponentially thin neighborhood of the cusp, specifically if $|\mu_n| \gtrsim \Delta_{\delta^{2/3}}$, or from (3.1) $|\mu_n| \gtrsim \exp[-1/\kappa\Omega\delta^{1/3}]$. However, our discussion of (3.1) is valid in any case, since if $|\mu_n| \lesssim \Delta_{\delta^{2/3}}$ in (3.1), then $|\mu_{n+1}| \gtrsim \delta^{-1/3}$, i.e., the next iterate is outside the range of the canonical analysis. To this extent it does not matter that (3.1) is *strictly* inaccurate near $\mu_n = 0$: it will give qualitatively and quantitatively a grossly true picture.

Since $\tilde{\rho}$ is proportional to $\rho - \rho_s$, as ρ varies, so also does $\tilde{\rho}$. Moreover, changing $\tilde{\rho}$ in (3.1) has the exact effect of moving the curve $\mu_{n+1}(\mu_n)$ up or down. This makes an exact analysis very easy. Note that the cusp (at $\mu_n = 0$) is due to the term $\ln|\mu_n|$ in (3.1), and therefore *without* this term, (3.1) represents a local approximation to the envelope curve. We assume the envelope has a (nonzero) stable fixed point (at $M_n \approx 1 + 1/4\rho_s$); then (since its local is $\mu_{n+1} \approx \tilde{\rho} + \kappa\mu_n$) this implies $\kappa < 1$. This is consistent with direct numerical integrations for computed values of κ at various δ; see Section 4. The form of

$$f(\mu) = \tilde{\rho} + \kappa(\mu - \Omega \ln|\mu|) \tag{3.2}$$

is then shown in Figure 5.

The first task is to evaluate the fixed points. Depending on $\tilde{\rho}$, there will be one, two, or three. Precisely, there is always exactly one positive fixed point given by

$$\mu \exp\left[\frac{(1-\kappa)\mu}{\kappa\Omega}\right] = \exp\left[\frac{\tilde{\rho}}{\kappa\Omega}\right]. \tag{3.3}$$

For $\mu < 0$, there can be two fixed points μ_1, μ_2 given by

$$\mu = \frac{-\kappa\Omega}{1-\kappa}\nu, \qquad \nu e^{-\nu} = \frac{1-\kappa}{\kappa\Omega}\exp\left[\frac{\tilde{\rho}}{\kappa\Omega}\right]; \tag{3.4}$$

these roots exist if $\nu e^{-\nu} < e^{-1}$, and this defines a *critical value of* $\tilde{\rho}$,

$$\tilde{\rho}_1 = \kappa\Omega\left[-1 + \ln\left(\frac{\kappa\Omega}{1-\kappa}\right)\right]. \tag{3.5}$$

If $\tilde{\rho} < \tilde{\rho}_1$, there are two negative roots, say $\nu_1 > \nu_2$; if $\tilde{\rho} > \tilde{\rho}_1$, there are none. The two roots disappear at $\tilde{\rho} = \tilde{\rho}_1$ in a *saddle-node bifurcation*; this bifurcation is a candidate for the intermittent transition to chaos [16]. To be more specific, for

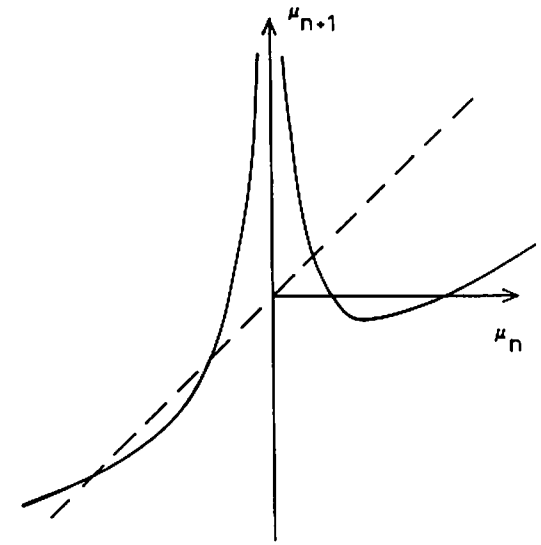

Figure 5. Form of $f(\mu)$ given by (3.2). Variations of $\tilde{\rho}$ have the effect of moving the μ_n-axis up and down.

$\tilde{\rho} < \tilde{\rho}_1$ the fixed point at $\mu = \mu_1$ represents a stable periodic solution in the $(s-1)$th trough T_{s-1} [between the $(s-1)$th and sth cusps]. As $\tilde{\rho}$ increases through $\tilde{\rho}_1$, the stable periodic orbit at μ_1 coalesces with the unstable one at μ_2 and is removed. Then motion in the $(s-1)$th trough is unstable, and iterates of μ_n make for the sth trough T_s. (We exclude the small possibility that μ_n enters a $\Delta_{\delta^{2/3}}$-neighborhood, though in this event, μ_n will get shifted up the envelope curve and "most probably" come back down to T_s again.) There is now the question what happens in T_s, which is in some sense "mostly" stable. Various possibilities (fixed point, chaos, etc.) can occur, but first we define more precisely when T_s will be stable, in the sense above.

Suppose $\tilde{\rho} < \tilde{\rho}_1$, so there are two negative fixed points of $f(\mu)$. By examining Figure 6, it is clear that motion in T_s can be stable, even when the stable fixed point μ_1 exists in T_{s-1}, if the minimum value of f for $\mu > 0$ ($= f_{\min}$) is less than the value of f at μ_2 ($= f_2$). One easily finds $f' = 0$ for $\mu = \Omega > 0$; therefore

$$f_{\min} = \tilde{\rho} + \kappa\Omega[1 - \ln\Omega]; \tag{3.6}$$

from (3.4) and (3.6), we find

$$f_{\min} - f_2 = \kappa\Omega\left[1 + \frac{\kappa\nu}{1-\kappa} + \ln\left(\frac{\kappa\nu}{1-\kappa}\right)\right]; \tag{3.7}$$

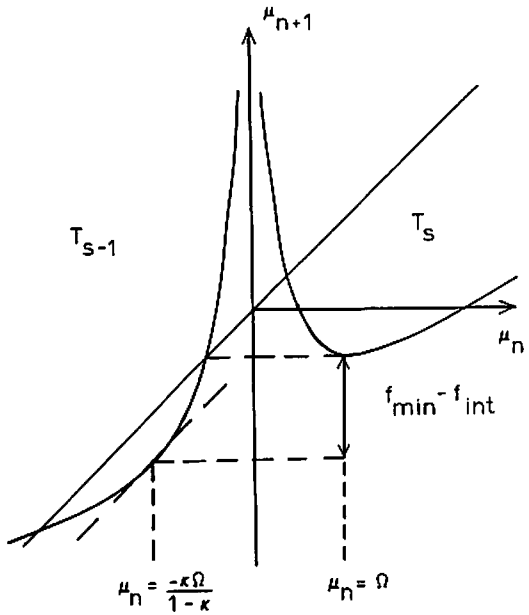

Figure 6. Equation (3.2) when $\tilde{\rho} = \tilde{\rho}_2$.

if we define ζ by

$$\zeta e^{\zeta} = e^{-1}, \qquad \zeta = 0.27846454\ldots, \tag{3.8}$$

then there is a critical value of $\tilde{\rho}$ ($= \tilde{\rho}_2$) when $f_{\min} - f_2 = 0$, i.e. when

$$\nu = \left(\frac{1-\kappa}{\kappa}\right)\zeta, \tag{3.9}$$

which since $f_2 = \mu_2 = f_{\min}$ at $\tilde{\rho} = \tilde{\rho}_2$, determines $\tilde{\rho}_2$ explicitly as

$$\tilde{\rho}_2 = -\Omega\zeta - \kappa\Omega(1 - \ln\Omega). \tag{3.10}$$

There is a criterion for $\tilde{\rho}_2$ to exist. By examining Figure 6, it is clear that this is that $f_{\min} > f_{\text{int}}$, where $f_{\text{int}} = f(\mu)$ when $\nu_1 = \nu_2$ ($= 1$). The criterion we derive is

$$f_{\min} - f_{\text{int}} > 0 \quad \text{if} \quad \frac{1}{1-\kappa} + \ln\left(\frac{\kappa}{1-\kappa}\right) > 0. \tag{3.11}$$

One can show that if κ satisfies (3.11), then $\nu < 1$ in (3.9), as required. If κ does *not* satisfy (3.11), stable behavior in the sth trough coexisting with the stable $(s-1)$

fixed point is less likely, though not impossible. Let us now assume (3.11) applies, i.e. $f_{\min} - f_{\text{int}} > 0$. This condition is equivalent to

$$\kappa > \frac{\zeta}{1+\zeta} \approx 0.2178117\ldots. \tag{3.12}$$

It is geometrically obvious (and can be proven) that if (3.12) holds, so that $\tilde{\rho}_2$ exists, then $\tilde{\rho}_1 > \tilde{\rho}_2$ for all $\kappa > \zeta/(1+\zeta)$. Therefore, as $\tilde{\rho}$ *increases*, for $\tilde{\rho} < \tilde{\rho}_2$, there is a stable (and an unstable) T_{s-1} fixed point; additionally, for $\tilde{\rho} < \tilde{\rho}_2$, motion within T_s is "unstable," in the sense that (certainly for sufficiently large $\tilde{\rho}_2 - \tilde{\rho}$) it will be chaotic, and then iterates of μ_n which visit the neighborhood of $\mu_n = \Omega$ will escape into T_{s-1}, and thence to the stable fixed point μ_1. For $\tilde{\rho}_2 < \tilde{\rho} < \tilde{\rho}_1$, T_s is essentially stable, in the sense that motions in T_s are necessarily bounded away from the fixed point in T_{s-1}; they may represent a fixed point, a p-cycle, or chaos, as for any (humped) difference map. We consider this further below. If for some n, $\mu_n \approx 0$, then a large excursion takes place to a higher trough, but generally further iterates will drift back down towards T_s again (see Figure 7).

For $\tilde{\rho} > \tilde{\rho}_1$, the two fixed points in T_{s-1} disappear in a saddle-node bifurcation and iterates of μ_n move towards T_s. If $f_{\min} - f_{\text{int}} < 0$ (i.e. $\kappa < 0.2178\ldots$), then (provided motion in T_s is chaotic) μ_n will be reinjected (for $\mu_n \approx \Omega$) to T_{s-1}, and intermittency [16] occurs. For $\kappa > 0.2178\ldots$, T_s is essentially stable, and one may enquire what happens to μ_n. One possibility is that the fixed point in $\mu > 0$ is stable. Clearly, the gradient there increases in absolute value as $\tilde{\rho}$ *decreases*. We can thus define a third critical value of $\tilde{\rho}$, when the fixed point is marginally

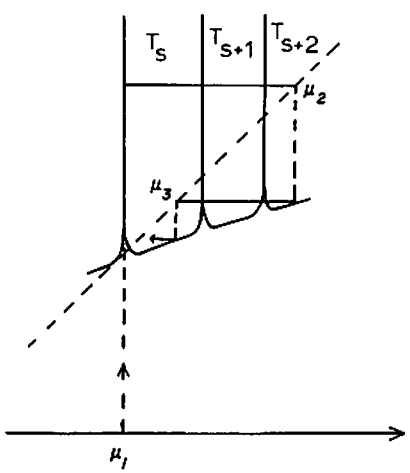

Figure 7. Occasionally iterates μ_n may "escape" near $\mu_n = 0$, but "mostly" they will drift back down towards T_s.

stable. This is when $f'(\mu)|_{\text{fixed point}} = -1$, and gives

$$\tilde{\rho}_3 = \kappa\Omega\left[\frac{1-\kappa}{1+\kappa} + \ln\left(\frac{\kappa\Omega}{1+\kappa}\right)\right]. \tag{3.13}$$

We find $\tilde{\rho}_3 > \tilde{\rho}_1$ if $\kappa < (1-\zeta)/(1+\zeta) \approx 0.5643765\ldots$. However, $\tilde{\rho}_3 > \tilde{\rho}_2$ for all $\kappa < 1$. As $\tilde{\rho}$ decreases below $\tilde{\rho}_3$, the positive fixed point of (3.1) bifurcates to a two-cycle, then to a four-cycle, etc., in the usual period-doubling manner. We say the system enters a *period-doubling window* [24]. Notice that this happens as $\tilde{\rho}$ *decreases*. If iterates of μ_n are restricted to T_s, then period doubling proceeds in a normal Feigenbaum manner, and there should exist a limiting value $\tilde{\rho}_\infty$ at which chaos occurs (there are infinitely many periodic solutions). We cannot give an exact estimate of this value; however, we can determine for what $\tilde{\rho}$ the "usual" period-doubling sequence will break down. This is when $f_{\min} \leqslant 0$, since then some iterates of μ_n will lie to the left of the cusp, i.e. on T_{s-1}. (A homoclinic explosion occurs when $f_{\min} = 0$.) This happens at a value $\tilde{\rho}_4 > \tilde{\rho}_2$ given by

$$\tilde{\rho}_4 = \kappa\Omega[\ln\Omega - 1]. \tag{3.14}$$

When $\tilde{\rho} = \tilde{\rho}_4$, iterates of $\mu_n > 0$ are governed by

$$\frac{\mu_{n+1}}{\Omega} = \kappa\left[\frac{\mu_n}{\Omega} - 1 - \ln\left(\frac{\mu_n}{\Omega}\right)\right]. \tag{3.15}$$

It seems plausible that as κ increases, (3.15) should take a period-doubling route to chaos at some limiting value κ^*. Then for $\kappa > \kappa^*$, we should have $\tilde{\rho}_\infty > \tilde{\rho}_4$ and the Feigenbaum period-doubling window would be completed before transition to T_{s-1} begins (at $\tilde{\rho}_4$). We can now summarize the results of this section in Figure 8.

We consider only the range $0 < \kappa < 1$, so that the envelope equation has a stable fixed point [at $\mu = \tilde{\rho}/(1-\kappa)$]. There are two principal bifurcation values of the parameter $\tilde{\rho}$. At $\tilde{\rho}_1$, a stable and an unstable fixed point in T_{s-1} coalesce and are extinguished as $\tilde{\rho}$ increases. If $\kappa < 0.2178$, there results an intermittent transition to T_s; this will be an *intermittent chaos* if the motion on T_s is chaotic. For $\kappa < 0.2178$, one has $\tilde{\rho}_3 > \tilde{\rho}_1$, and in fact $\tilde{\rho}_4 > \tilde{\rho}_1$; therefore, if the conjecture above is correct, and if $\kappa^* < 0.2178$, then intermittent chaos will *certainly* occur for $\tilde{\rho} = \tilde{\rho}_1 +$ if $\kappa^* < \kappa < 0.2178\ldots$. If $\kappa > 0.2178\ldots$, then the saddle-node bifurcation at $\tilde{\rho}_1$ is not intermittent, since the motion switches to stable behavior on T_s. If $\kappa < 0.5$, we have $\tilde{\rho}_4 > \tilde{\rho}_1$, and if $\kappa > \kappa^*$, then we should observe chaos on T_s. As $\tilde{\rho}$ increases further (this is also true for $\kappa < 0.2178\ldots$), the chaotic motion is transformed through an inverse period-doubling window starting somewhere above $\tilde{\rho}_4$ to a stable fixed point for $\tilde{\rho} > \tilde{\rho}_3$. If $\kappa < 0.2178\ldots$, T_s is stable (intermittency ceases) when $\tilde{\rho} > \tilde{\rho}_4$. If $0.5 < \kappa < 0.5643\ldots$, the motion at $\tilde{\rho}_1 +$ on T_s may not be chaotic, and if $\kappa > 0.5643\ldots$, then $\tilde{\rho}_3 < \tilde{\rho}_1$, and the transition at $\tilde{\rho}_1$ is from a stable T_{s-1} fixed point to a stable T_s fixed point. As $\tilde{\rho}$ increases, the stable T_s fixed point will coalesce with an unstable T_s fixed point in a further saddle-node bifurcation near the $(s+1)$th cusp.

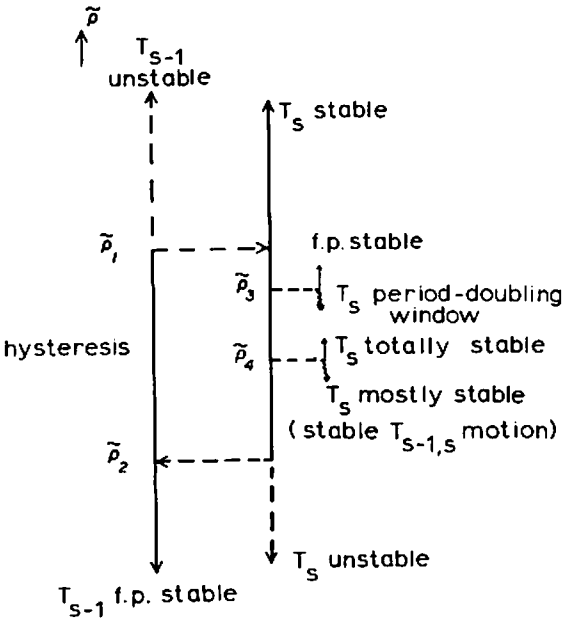

(a) $\kappa = 0.2178\ldots$

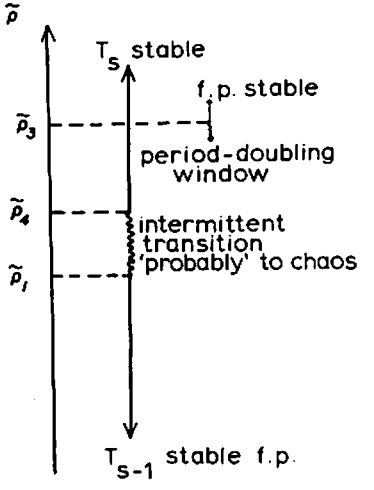

(b) $\kappa = 0.2178\ldots$

Figure 8. (a) $\kappa > 0.2178\ldots$. The hysteresis path is shown by the dashed arrows between the T_{s-1} and T_s tracks. $\tilde{\rho}_3 > \tilde{\rho}_1$ if $\kappa < 0.5643\ldots$; $\tilde{\rho}_4 > \tilde{\rho}_1$ if $\kappa < 0.5$. The period-doubling window will "probably" lie in $(\tilde{\rho}_4, \tilde{\rho}_3)$ (if $\tilde{\rho}_4 < \tilde{\rho}_3$). (b) $\kappa < 0.2178\ldots$. The intermittent transition at $\tilde{\rho}_1$ is "probably" to chaos—though possibly to a periodic solution. Continuity between (a) and (b) is because $\tilde{\rho}_1 = \tilde{\rho}_2$ there.

If $\kappa > 0.2178$, there is a further bifurcation value $\tilde{\rho}_2 < \tilde{\rho}_1, \tilde{\rho}_4, \tilde{\rho}_3$, at which T_s becomes unstable. Properly, this is (at $\tilde{\rho}_2$-) only to chaotic motions on T_s, since only these can be guaranteed to visit the neighborhood of the minimum of μ_{n+1} at $\mu_n = \Omega$, and hence pass towards T_{s-1} and its stable fixed point. Again, since $\tilde{\rho}_4 > \tilde{\rho}_2$, it is likely (if $\kappa > \kappa^*$ also) that T_s really is unstable at $\tilde{\rho}_2$-, although in any case the instability is enhanced as $\tilde{\rho}$ decreases. In this case ($\kappa > 0.2178\ldots$), we see that there is a phenomenon of *hysteresis* in the range $\tilde{\rho}_2 < \tilde{\rho} < \tilde{\rho}_1$, as observed previously by Fowler and McGuinness [4]. We also see that *hysteresis* and *intermittency* appear as *complementary* phenomena in this context: the one precludes the other. This may have some physical significance.

4. Application to the Lorenz system

It is fairly straightforward to compute the values of the bifurcation parameter r at the various transitions described in the previous section. Before presenting these, let us make a comment on the expected accuracy of the results. The difference equation we consider is formally accurate to $O(\delta^{4/3})$; since the cusp spacing is $O(\delta^{2/3})$, this means that the values $\rho_{(s)}$ at which the sth cusp overlies the fixed point (and near which transition occurs) are accurate to $O(\delta^{2/3})$. With $r_{(s)} = \sigma\rho_{(s)}$ being the corresponding transition value of r, this means $r_{(s)}$ is formally accurate to $O(\sigma^{1/3}) \approx 8$ for $\sigma = 500$. However, "$O(1)$" constants which are numerically large can widen this limit of accuracy, and such large numbers abound in the Lorenz computations. For example, we have (with $\bar{\gamma} = 1$) $a = 5.404$, $\theta = 3.29$, $\bar{\rho}/\tilde{\rho} \sim 10$, $D^* = 5.327$, and so on. This means that the relative correction term of $O(\delta)$ in the difference equation may not be *numerically* small compared to $O(\delta^{2/3})$ unless, say, $10\delta^{1/3}$ is small. This would require $\sigma \gtrsim 10^5$; however, direct numerical integration becomes tortuous even at $\sigma = 500$ (floating underflow errors occur in single precision, due to the smallness of x in the slow phase), and in any case the cusp spacing would then be $\lesssim 10^{-3}$ on a zero-to-one scale—prohibitively small. It seems pointless to try to gain better numerical accuracy at the cost of excessive computing time, when the major point of our analysis is to explain and illustrate the observed behavior of the Lorenz system at high, but not enormous, Prandtl number. With this proviso, we take the numerical accuracy claimed in the abstract to be relative numerical accuracy, and proceed with the results.

Results of direct numerical integrations of the equations are shown in Tables 1–4. A fourth-order fixed-stepsize Runge-Kutta iteration was used to integrate the Lorenz equations on a CDC CYBER 203. Single-precision arithmetic was used (64-bit words), and the stepsize was chosen to be $0.1/D$, where $D = \max(r, \sigma)$. A comparison of a typical result from Tables 2, 3, 4 with the result obtained using a stepsize of half the above value gave agreement to four places after the decimal point. The uncertainty in the results in Tables 2, 3, 4 is not more than ± 0.0001. The notation in the tables is as follows: T_s indicates a solution in the sth trough ($T_{s,s+1}$ indicates a solution partly in T_s and partly in T_{s+1}, i.e. for which $\tilde{\rho}_2 < \tilde{\rho} < \tilde{\rho}_4$ in the notation of Section 3). Numbers represent values of M_n, f.p. denotes fixed point, ap.m. denotes aperiodic motion, and $1.38 \leftrightarrow 1.42$ indicates the *range*—e.g., 2-cycle $1.38 \leftrightarrow 1.42$ is a 2-cycle of the difference equation between 1.38 and 1.42., (i.e., M_n takes successive values 1.38, 1.42, 1.38,...), and so on. It

is evident on examination of Tables 1–4 that the analysis of Section 3 is consistent with the numerical results. We see hysteresis for $\sigma \geqslant 50$, and narrow period-doubling windows as r *decreases* near transition values. Since the solution in the lower trough near transition is always a fixed point, this suggests $\kappa < 1$. Hysteresis suggests $\kappa > 0.2178\ldots$, and the apparent existence of concurrent fixed points on T_s and T_{s+1} suggests $\kappa > 0.5643\ldots$ (at least for the higher values of σ). Identification of Figure 6(a) with the tables requires $\tilde{\rho}/\bar{\rho}$ to be positive, as it is in fact computed to be. We list, in Tables 5–8, the computed values of the transition parameters for $\sigma = 50, 100, 300, 500$; the results are given both when the $O(\delta)$ terms are included and when they are omitted. The cusp number l is associated with transition from T_{l-1} to T_l.

There are several points to note from these tables. We have already commented on the largeness of some of the "order one" numbers. Particularly, defining $\bar{\rho}/\tilde{\rho} = X$, we find that although formally $X = O(1)$, numerically X can be quite large. Obviously, the analysis cannot be expected to be accurate when $X \sim \sigma$, and

Table 1

σ	r	Solutions
50	95	T_1 f.p. ≈ 1.2535
	100	T_1 f.p. ≈ 1.25
		T_2 ap.m. $1.3 \leftrightarrow 1.4$

Table 2
$\sigma = 100$

r	Solutions
110	T_1 f.p.
	T_2 ap.m.
111	T_1 f.p. 1.338
	T_2 4-cycle $1.38 \leftrightarrow 1.42$
113	T_1 f.p. 1.339
	T_2 2-cycle 1.39, 1.41
114	T_1 f.p. 1.3431
	T_2 2-cycle 1.38, 1.40
115	T_2 2-cycle 1.38, 1.39
116	T_2 f.p. 1.3836
200	T_2 f.p. 1.279
	$T_{2,3}$ ap.m. $1.31 \leftrightarrow 1.34$
500	$T_{2,3,4}$ ap.m. $1.19 \leftrightarrow 1.23$
1000	T_2 2-cycle 1.107, 1.096

we have indicated with an exclamation mark (!) cusp numbers in Tables 5–8 for which $X/\sigma > 0.2$. Values for which $X/\sigma < 0$ (and in fact < -0.2) are indicated by two exclamation marks (!!). One can show that, for each s, X is inversely proportional to $(dC/d\rho)_{\rho_s}$, where $C(\rho)$ is the fixed point of the envelope curve. Thus $X \to \infty$ as C becomes stationary; in other words, the tables show that the cusps first move to the left as ρ increases (fixed point moves to the right, $dC/d\rho > 0$, $X > 0$), but then $1/X$ passes through zero, and they start to move to the left. This can be clearly seen in the numerical results of Tables 2–4.

Table 3
$\sigma = 300$

r	Solutions	r	Solutions
220	T_1 f.p. 1.3856	340	T_4 f.p. 1.3806
225	T_1 f.p. 1.3795	350	T_4 f.p. 1.375
230	T_1 f.p.		$T_{4,5}$ ap.m. 1.39 ↔ 1.41
	$T_{1,2}$ ap.m. 1.41 ↔ 1.43	360	T_4 f.p. 1.3705
239	T_1 f.p.		T_5 ap.m. 1.40 ↔ 1.39
	T_2 2-cycle 1.4099, 1.4090	370	T_5 2-cycle 1.382, 1.384
240	T_1 f.p. 1.3663	380	T_5 f.p. 1.3766
	T_2 f.p. 1.4082	410	T_5 f.p. 1.3599
246	T_1 f.p. 1.3644	420	T_5 f.p. 1.3553
	T_2 f.p. 1.4012		$T_{5,6}$ ap.m. 1.381 ↔ 1.371
250	T_2 f.p. 1.3970	430	T_5 f.p. 1.3511
260	T_2 f.p. 1.3881		$T_{5,6}$ ap.m. 1.38 ↔ 1.36
	$T_{2,3}$ ap.m. 1.44 ↔ 1.42	440	T_5 f.p. 1.3476
270	T_2 f.p. 1.3824		T_6 ap.m. 1.378 ↔ 1.362
	T_3 2-cycle 1.4139, 1.4093	450	T_5 f.p. 1.3458
280	T_3 f.p. 1.4010		T_6 2-cycle 1.3626, 1.3569
310	T_3 f.p. 1.3813	455	T_6 2-cycle 1.3553, 1.3576
	T_4 2-cycle 1.401, 1.407	460	T_6 f.p. 1.3538
312	T_3 f.p. 1.3812	480	T_6 f.p. 1.3445
	T_4 2-cycle 1.4010, 1.4018	600	T_6 f.p. 1.3040
313	T_3 f.p. 1.3814		T_7 ap.m. 1.327 ↔ 1.317
	T_4 f.p. 1.4005	700	T_7 f.p. 1.2889
314	T_3 f.p. 1.3822	1000	T_7 f.p. 1.2333
	T_4 f.p. 1.3997	2000	T_6 f.p. 1.1452
315	T_4 f.p. 1.3988		

Table 4
$\sigma = 500$

r	Solutions	r	Solutions
400	T_2 f.p. 1.3860	555	T_6 f.p. 1.3859
	T_3 ap.m. 1.421 ↔ 1.410		T_7 2-cycle 1.403, 1.397
420	T_3 f.p. 1.3984	560	T_6 f.p. 1.3949
440	T_3 f.p. 1.3920		T_7 2-cycle 1.3951, 1.3983
	T_4 f.p. 1.4076	565	T_7 f.p. 1.3941
460	T_4 f.p. 1.3970	600	T_7 f.p. 1.3801
	$T_{4,5}$ 4-cycle 1.419 ↔ 1.413	650	T_8 f.p. 1.3940
480	T_5 f.p. 1.4035	700	T_8 f.p. 1.361
510	T_5 f.p. 1.3915		T_9 2-cycle 1.368, 1.371
512	T_5 f.p. 1.3913	800	T_9 f.p. 1.342
	T_6 f.p. 1.4039		T_{10} 8-cycle 1.356 ↔ 1.350
514	T_5 f.p. 1.3917	900	T_{10} f.p. 1.3271
	T_6 f.p. 1.4028	1000	T_{11} 2-cycle 1.3177, 1.3155
515	T_6 f.p. 1.4023	1100	T_{11} f.p. 1.2985
520	T_6 f.p. 1.3997	1200	T_{11} f.p. 1.2835
540	T_6 f.p. 1.3907	2000	$T_{1,10}$ 2-cycle 1.2011, 1.2086
550	T_6 f.p. 1.3875	2100	$T_{1,10}$ 2-cycle 1.1951, 1.2026
	$T_{6,7}$ ap.m. 1.399 ↔ 1.411		

Table 5
$\sigma = 50$

Accuracy	Cusp location	Cusp number	r_1	r_2	r_3	r_4	κ
$O(\delta^{2/3})$	1.39	! 1	90.5	29.9	75.2	57.8	0.63
		2	Transition values do not exist				
$O(\delta)$	1.26	! 1	41.0	35.7	51.9	48.7	0.40
		2	Transition values do not exist				
$O(\delta)^*$		1	30.9	30.1	35.0	34.4	0.34
		! 2	16.7	5.9	86.3	77.4	0.33

Tables 5 and 6 show three sets of figures: $O(\delta^{2/3})$, $O(\delta)$, and $O(\delta)^*$. The $O(\delta^{2/3})$ results are computed from (2.19) and (2.21), where we ignore $O(\delta)$ in solving (2.16). The $O(\delta)^*$ results include the $O(\delta)$ terms in (2.16); the $O(\delta)$ results do as well, but with the exception that we use $D = D(\bar{\gamma}, m, \rho)$, $m = 2 - C_v$, rather than $D = D^*$, $m = 1 - 1/4\rho$. One can see that the difference between the different results is substantial at these comparatively low values of σ. There is no particular reason to choose one or other $O(\delta)$ result for comparison with numerical experiment, except to juggle with the accuracy, and in Tables 7 and 8 we have used the $O(\delta)$ results. One can see a substantial difference between these and the $O(\delta^{2/3})$ results.

Table 6
$\sigma = 100$

Accuracy	Cusp location	Cusp number	r_1	r_2	r_3	r_4	κ
$O(\delta^{2/3})$	1.41	1	108.5	76.5	92.4	85.6	0.73
	1.38	! 2	189.6	81.8	168.6	136.2	0.61
$O(\delta)$	1.38	1	73.1	66.9	74.1	71.8	0.53
	1.31	! 2	120.1	90.0	134.9	121.9	0.49
$O(\delta)^*$		1	64.8	61.0	66.2	64.6	0.51
		2	87.5	80.8	94.1	90.7	0.45
		! 3	111.7	73.3	164.3	143.3	0.43

Table 7
$\sigma = 300$

Accuracy	Cusp location	Cusp number	r_1	r_2	r_3	r_4	κ
$O(\delta^{2/3})$	1.39	1	271.7	221.3	233.8	227.6	0.90
	1.41	2	274.6	241.8	255.8	249.5	0.77
	1.41	3	302.1	268.9	287.5	279.7	0.70
	1.40	4	343.7	301.8	329.9	318.7	0.65
	1.39	5	407.9	338.9	391.7	371.6	0.62
	1.36	! 6	566.4	334.9	529.7	458.1	0.60
	1.32	!! 7	471.2	681.4	492.5	560.2	0.59
$O(\delta)$	1.40	1	218.5	198.9	206.9	203.2	0.78
	1.40	2	240.5	223.6	233.6	229.4	0.68
	1.40	3	271.5	252.6	266.5	261.1	0.63
	1.39	4	312.2	287.0	308.5	300.6	0.60
	1.37	5	369.8	327.1	367.6	353.3	0.58
	1.34	! 6	481.6	346.2	484.8	437.5	0.56
	1.29	!! 7	504.4	665.3	492.9	550.6	0.55

The main content of the results is given in Tables 7 and 8, for $\sigma = 300$ and 500. To compare these predictions with numerical experiment, observe that for a given cusp number s, the predicted behavior is (with $\kappa > 0.56\ldots$, as it mostly is)

(i) $r < r_2$: T_{s-1} f.p.
(ii) $r_2 < r < r_4$: T_{s-1} f.p.; $T_{s-1,s}$ ap.m.
(iii) $r_4 < r < r_3$: T_{s-1} f.p.; T_s p.d.w. (period-doubling window).
(iv) $r_3 < r < r_1$: T_{s-1} f.p.; T_s f.p.
(v) $r > r_1$: T_s f.p.

These predictions are in moderately good quantitative agreement with the numerical results. For example, we see the above sequence of five behaviors (for $s = 5$, $\sigma = 300$) at r values:

(i) 340;
(ii) 350;
(iii) 360;
(iv) 370 (T_4 f.p. missing, though);
(v) 380.

Table 8
$\sigma = 500$

Accuracy	Cusp location	Cusp number	r_1	r_2	r_3	r_4	κ
$O(\delta^{2/3})$	1.38	1	455.4	370.5	383.5	376.8	0.97
	1.40	2	425.5	384.9	397.4	391.4	0.85
	1.41	3	440.3	406.7	420.4	414.1	0.78
	1.41	4	464.8	432.9	448.7	441.9	0.73
	1.41	5	496.7	463.1	482.3	474.3	0.69
	1.41	6	535.7	497.5	521.9	512.1	0.66
	1.40	7	583.5	536.6	569.5	556.6	0.64
	1.39	8	644.7	580.4	629.1	610.5	0.62
	1.38	9	731.5	625.1	710.7	678.7	0.61
	1.36	! 10	917.5	617.8	871.9	778.8	0.60
$O(\delta)$	1.39	1	376.2	341.0	350.3	345.8	0.88
	1.40	2	385.8	361.5	371.2	366.8	0.78
	1.41	3	407.8	386.0	397.0	392.2	0.72
	1.41	4	435.6	413.6	426.6	421.3	0.68
	1.40	5	468.7	444.8	460.8	454.5	0.65
	1.40	6	507.7	479.9	500.5	492.6	0.63
	1.39	7	554.7	519.9	547.8	537.4	0.61
	1.38	8	612.9	564.9	606.2	591.2	0.60
	1.36	9	691.9	613.0	684.8	659.2	0.58
	1.34	! 10	837.1	627.4	827.2	757.1	0.57

These can be compared with the predicted ranges of r:

(i) $r < 327.1$;
(ii) $327.1 \rightarrow 353.3$;
(iii) $353.3 \rightarrow 367.6$;
(iv) $367.6 \rightarrow 369.8$ (very narrow as κ is close to 0.56, perhaps explaining the absence of a T_4 f.p. at 370);
(v) $r > 369.8$.

We might also note that X increases with s, so that lower values of s might be expected to be more accurate.

Comparing Tables 4 and 8, we see similar broad agreement, although mostly one sees fixed points. For example the $T_6 \rightarrow T_7$ transition occurs within the interval (540, 565) as compared to the predicted (519.9, 554.7). Compilation of tables such as these requires a great deal of laborious numerical work, and comparison of prediction and observation inevitably suggests further parameter values for study. However, we think that, at least in a large-scale manner, we have a suitable explanation for most of the behavior which we have observed.

To indicate that all is not completely resolved, we may point out the anomalous $T_{1,10}$ and $T_{2,3,4}$ modes in Tables 4 and 2, respectively. The $T_{1,10}$ 2-cycle suggests that an extra maximum of Z occurs before the slow exponential decay, and this is consistent with the increase in frequency ω of the oscillatory decay in the fast phase [4] as ρ increases, and with the transition to the high-r limit cycle, which is (essentially) dominated by this frequency. $T_{2,3,4}$ motion might be similarly understood: we have not pursued these ideas.

We may notice from the tables that $r_{(1)} < \sigma$, so that stable T_1 behavior first appears at subcritical r (below the linear-stability limit). This corresponds to the case for Lorenz's parameters $\sigma = 10$, $b = \frac{8}{3}$, when stable $T_{0,1}$ behavior appears at $r = 24.06\ldots < 24.74 =$ the linear stability limit [10]. This corresponds to $\tilde{\rho} > \tilde{\rho}_2$ for cusp number 1 (if $\kappa > 0.21\ldots$). We can compute the corresponding r-values, r_A say, in various ways. We have $r_A/\sigma = \rho_A = \rho_{(1)} + \delta X \tilde{\rho}_2$. If we completely neglect δ, then we find $\rho_A \approx 0.822$. For $200 \lesssim \sigma \lesssim 700$, we find $\rho_{(1)}$ to $O(\delta^{2/3})$ *decreasing* to about 0.76, where it seems about to start increasing. $\rho_{(1)}$ to $O(\delta)$ is slowly increasing to about 0.71. Including $\tilde{\rho}_2$ and $O(\delta)$ terms shows ρ slowly increasing to about 0.70 at $\sigma = 700$. The best we can probably say is that the critical value r_A, at which the strange invariant set becomes attracting, is such that r_A/σ is a slowly varying function of σ with $r_A/\sigma \sim 0.7$ for $\sigma \sim 500$, and $r_A/\sigma \rightarrow 0.82$ as $\sigma \rightarrow \infty$. Additionally, we know the linear stability limit $r_T \approx \sigma$, and since the first cusp is located at $M_n \approx 1 + 1/4\rho$, the first homoclinic explosion occurs (i.e. the strange invariant set is born) when $M_n \approx 2$, i.e. $\rho \sim 0.25$; the corresponding value of r, r_S, then satisfies $r_S \approx 0.25\sigma$. Thus the three curves in (σ, r) parameter space corresponding to linear stability of the fixed points, existence of a strange attractor, and existence of a strange invariant set should have slopes ≈ 1, 0.82, and 0.25 respectively. An examination of Figure 4 in the paper by Robbins [21] indicates that this prediction is qualitatively reasonably accurate for $\sigma \gtrsim 10$.

5. Conclusions

From an analytically derived difference equation for the Lorenz system, we obtain a canonical difference equation (some of) whose bifurcation behavior can be explicitly analysed. We are able to predict complementary phenomena of intermittency (saddle-node bifurcation in which a stable and an unstable limit cycle coalesce) and hysteresis; the latter seems preferred at higher Prandtl number, and produces multiple (two) stable behaviors at a single set of parameter values. We are also able to predict period-doubling behavior as r decreases, as numerically observed. The analysis is successful in the sense that many different phenomena are explained in a satisfactory qualitative manner, but the quantitative results could be more accurate. As previously discussed, we consider such numerical discrepancies as exist to be due to the crudity of the approximation: to reduce these, one would have to take such high values of σ that the principal features of the derived difference equation would become difficult to visualize. We have not attempted to do this, since the present results demonstrate the applicability of the analysis in a real qualitative sense.

References

1. M. Abramowitz and A. Stegun, *Handbook of Mathematical Functions*, Dover, New York, 1968.
2. J. C. Antoranz, J. Gea, and M. G. Velarde, Oscillatory phenomena and Q switching in a model for a laser with a saturable absorber, *Phys. Rev. Lett.* 47:1895–1898 (1981).
3. P. Collet and J.-P. Eckmann, *Iterated Maps on the Interval as Dynamical Systems*, Birkhäuser, Basel, 1980.
4. A. C. Fowler and M. J. McGuinness, A description of the Lorenz attractor at high Prandtl number, *Physica D*, to appear.
5. A. G. Fox, S. E. Schwarz, and P. W. Smith, Use of neon as a nonlinear absorber for mode locking a He-Ne laser, *Appl. Phys. Lett.* 12:371–373 (1968).
6. J. D. Gibbon and M. J. McGuinness, A derivation of the Lorenz equations for some unstable dispersive physical systems, *Phys. Lett.* 77A:295–299 (1980).
7. J. Guckenheimer and R. F. Williams, Structural stability of Lorenz attractors, *Publ. I.H.E.S.* 50:307–320 (1979).
8. H. Haken, Analogy between higher instabilities in fluids and lasers, *Phys. Lett.* 53A:77–78 (1975).
9. P. L. Hanst, J. A. Morreal, and W. J. Henson, Repetitive pulsing of the CO_2 laser by means of CO_2 gas and other absorbers, *Appl. Phys. Lett.* 12:58–61 (1968).
10. J. L. Kaplan and J. A. Yorke, Preturbulence: a regime observed in a fluid flow model of Lorenz, *Comm. Math. Phys.* 67:93–108 (1979).
11. P. H. Lee, P. B. Schoeffer, and W. B. Barber, Single-mode power from a 6328 Å laser incorporating neon absorption, *Appl. Phys. Lett.* 13:373–375 (1968).
12. M. Levi, Qualitative analysis of the periodically forced relaxation oscillations, *Mem. Amer. Math. Soc.* 32, No. 244 (1981).
13. E. N. Lorenz, Deterministic non-periodic flow, *J. Atmospheric Sci.* 20:130–141 (1963).
14. E. N. Lorenz, On the prevalence of aperiodicity in simple systems, *Global Analysis* (M. Grmela and J. E. Marsden, Eds.), Springer, Berlin, 1979, pp. 53–75.
15. P. Manneville and Y. Pomeau, Intermittency and the Lorenz model, *Phys. Lett.* 75A:1–2 (1979).
16. P. Manneville and Y. Pomeau, Different ways to turbulence in dissipative dynamical systems, *Physica* 1D:219–226 (1980).
17. J. Maurer and A. Libchaber, Effect of the Prandtl number on the onset of turbulence in liquid ^{4}He, *J. Phys. Lett.* 41:L515–L518 (1980).

18. R. M. May,. Simple mathematical models with very complicated dynamics, *Nature* 261:459–467 (1976).
19. N. Morioka and T. Shimizu, Transition between turbulent and periodic states in the Lorenz model, *Phys. Lett.* 66A:447–449 (1978).
20. O. Reynolds, On the experimental investigation of the circumstances which determine whether the motion of water shall be direct or sinuous, and the law of resistance in parallel channels, *Philos. Trans. Roy. Soc.* 174:935–982 (1883).
21. K. A. Robbins, A new approach to subcritical instability and turbulent transitions in a simple dynamo, *Math. Proc. Cambridge Philos. Soc.* 82:309–325 (1977).
22. K. A. Robbins, Periodic solutions and bifurcation structure at high R in the Lorenz model, *SIAM J. Appl. Math.* 36:457–472 (1979).
23. H. Schlichting, *Boundary Layer Theory*, McGraw-Hill, New York, 1980.
24. T. Shimizu, Analytic form of the simplest limit cycle in the Lorenz model, *Physica* 97A:383–398 (1979).
25. C. Sparrow, The Lorenz equations: bifurcations, chaos, and strange attractors, *Appl. Math. Sci.* 41, Springer, Berlin, 1982.
26. C. Tresser, P. Coullet, and A. Arneodo, On the existence of hysteresis in a transition to chaos after a single bifurcation. *J. Phys. Lett.* 41:L243–L246 (1980).
27. J. A. Yorke and E. D. Yorke, Metastable chaos: the transition to sustained chaotic behavior in the Lorenz model, *J. Statist. Phys.* 21:263–277 (1979).

Massachusetts Institute of Technology
California Institute of Technology

(Received July 23, 1982)